Mount for a large potassium bromide beamsplitter in a cryogenic, space application

Gregory L. Klotz

Jet Propulsion Laboratory, California Institute of Technology
MS 158/224, Pasadena, CA 91109

ABSTRACT

This paper describes an approach to mounting Potassium Bromide (KBr) optical elements that are expected to survive launch vibrations and a cryogenic environment. These KBr optics constitute the beamsplitter and compensator for a high-resolution, infrared Fourier transform spectrometer (FTS). This spectrometer is part of the Tropospheric Emissions Spectrometer (TES) instrument which will operate in the 3.2 to15.4 μm spectral range. TES is part of NASA's Earth Observing System (EOS) initiative to better understand our Earth's environment. TES is designed to obtain data on tropospheric ozone and other gas molecules that lead to ozone formation. These data will be used to create a three-dimensional model describing the global distribution of these gases to better understand global warming and ozone depletion. TES uses a Connes interferometer where the clear aperture (CA) responsible for splitting the science beam is distinct and separated by 108 mm from the CA which recombines the split beams.

KBr has a low elastic limit and a high coefficient of thermal expansion, is highly soluble in water and is susceptible to degradation from humidity. These characteristics make it a rather difficult optical material to mount and protect from environments typically resisted by glass optics. The design described here uses a diameter to thickness aspect ratio of 6:1 (based on a 190 mm diameter) resulting in a rather massive element. Due to instrument mass and volume constraints in the interferometer, a pseudo-rectangular shape for the optical elements was devised and a graphite/cyanate ester support structure was designed to minimize the mass of the entire beamsplitter assembly.

Vibration isolation of the optical elements was provided by RTV silicone pads, which were also designed to meet thermal stress concerns for the 180K operating environment. Both structural and thermal analyses were performed to verify the initial design. Further vibration and thermal testing of development units is expected to uncover any unforeseen problems and to verify compliance in areas of concern.

This paper addresses RTV silicone material properties required to properly support the KBr optics and predicted KBr stresses and RTV preloads and deflections derived from an analytical model of the design configuration. Results from thermal and vibration testing of development units will also be presented (if available) and compared to preliminary thermal and structural models.

Keywords: potassium bromide, RTV silicone, cryogenic, optical mount, infrared, analytical model, space application

1. BACKGROUND

The Tropospheric Emissions Spectrometer (TES), selected for flight on the EOS-Chemistry1 mission, will provide the first global view of the chemical state of the troposphere (the lowest region of the atmosphere, extending from the surface to about 10-15 km altitude). The investigation will focus on mapping the global distribution of tropospheric ozone and on understanding the factors that control ozone concentrations. Ozone precursor gases of interest emit in the IR from 3.2 to 15.4 μm, and the TES interferometer metrology laser operates at 1.06 μm. The TES interferometer is a Connes type and because of the need for accuracy in this spectral range, the beamsplitter material of choice requires high transmissivity and low absorptivity throughout the range. Thus, the firm requirement for a potassium bromide (KBr) beamsplitter. This and other instrument science requirements as established by the science team are detailed in the TES science requirements document[1].

1.1. The instrument

Figure 1 illustrates the current TES optical bench configuration and Figure 2 is a schematic of the science and metrology beam optical paths. The interferometer optics begin with a fold mirror (M7) which reflects the science beam toward the first surface of the beamsplitter element at Level 1. The second surface of the beamsplitter is coated for 50/50 T/R. The beam that reflects off the coated surface continues (via the beamsplitter first surface) to roof mirrors M8-2 and M9-2, to the cube corner retroreflector (CC-2) and returns via Level 2 to the beamsplitter first surface. After traversing the beamsplitter, the beam is reflected back through the beamsplitter from its second surface (the recombiner CA) and continues on to the focal plane subsystem (FPS-2) via fold mirror M10-2.

Similarly, the original science beam which entered at M7 and was instead transmitted at the beamsplitter second surface, traverses the compensator, continues on to roof mirrors M8-1 and M9-1, on to CC-1, returns via Level 2 through the compensator and is recombined at the beamsplitter second surface with the beam described previously. The two interfering beams continue on through the beamsplitter and are finally imaged at the detector in FPS-2 via M10-2. The paths to FPS-1 are identical up to the recombination at the beamsplitter second surface except that the beams returning to the beamsplitter recombiner CA via Level 2 are the transmitted beam from Side 2 of the interferometer and the reflected beam which traversed Side 1.

This description is important to demonstrate the complexity of the TES interferometer and the requirement that the beamsplitter element contain two distinct clear apertures - a splitting CA and a recombining CA. Since the split beams are not recombined until shortly before they continue onto the M10 fold mirrors, these distinct clear apertures at the beamsplitter second surface must be coplanar to within $\lambda/4$ at 632.8 nm.

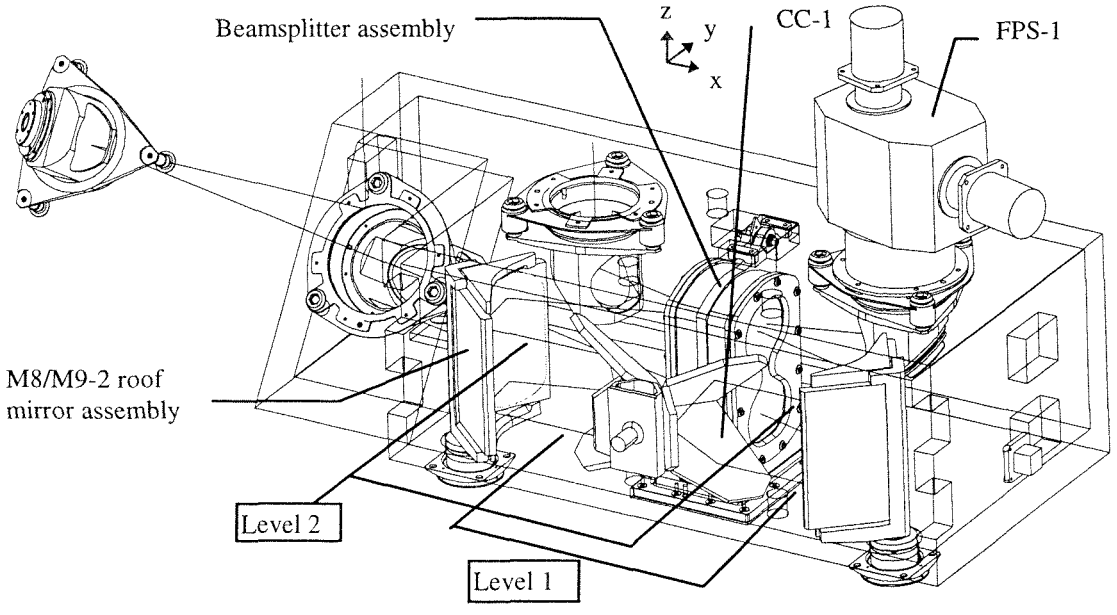

Figure 1. The TES optical bench showing the primary components, Level 1 (lower), Level 2 (upper) and sides -1 and -2 of the interferometer. FPS-2 is not shown, however, M10-1 and -2 fold mirrors assemblies are. The instrument coordinate system is also indicated.

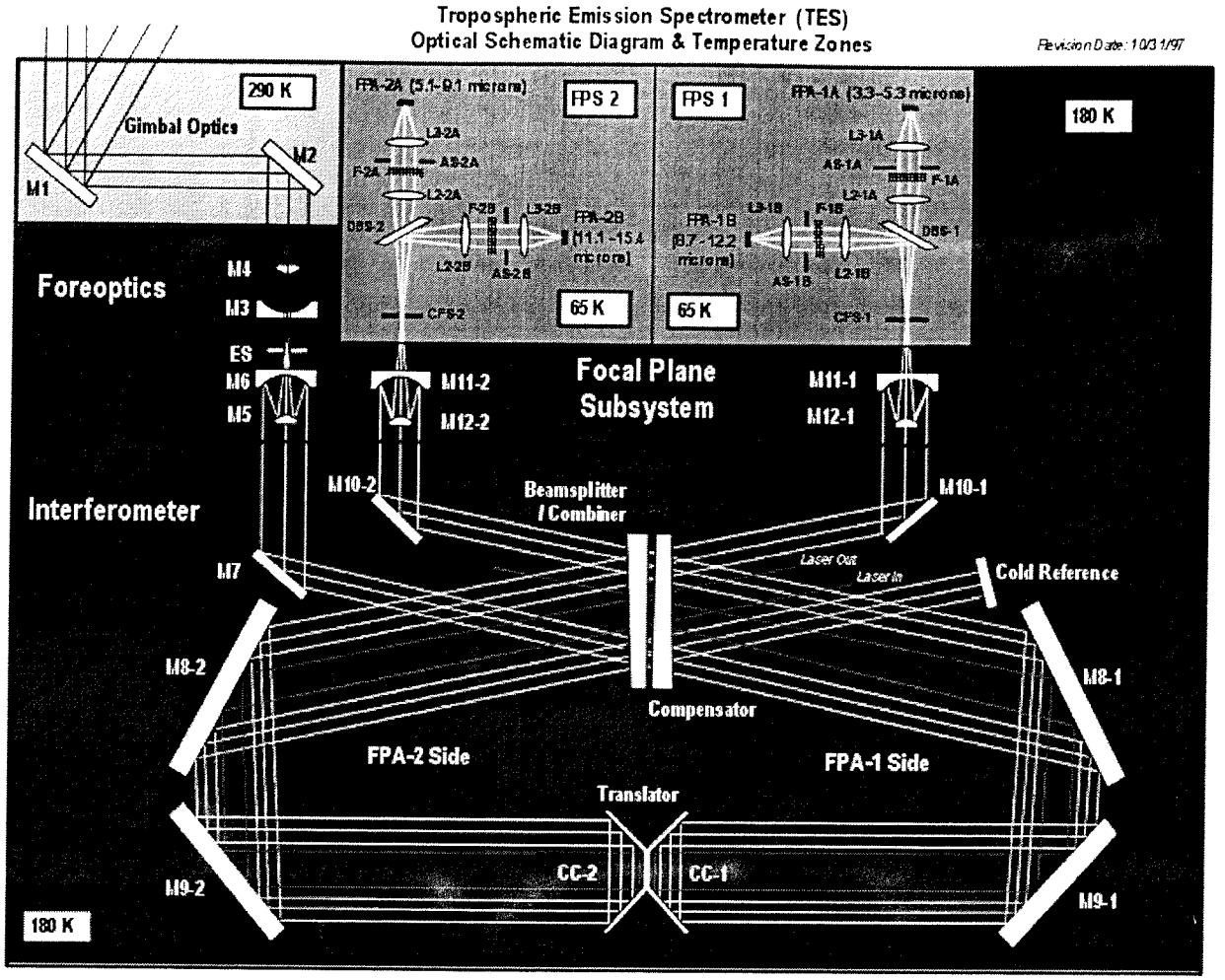

Figure 2. Diagram indicating the primary TES instrument optical paths and optical components. CC-1 and -2 are back-to-back Beryllium cube corner retroreflectors, M8 & M9 pairs are Be mirrors fabricated as a set and designated as roof mirrors, M7 folds the science beam into the interferometer and the M10 mirrors fold into the focal planes. The laser metrology path starts as a fiber/lens launcher and returns to a fiber/detector receiver (laser out) as indicated. A laser dump captures the remaining laser light between the beamsplitter and M10-2.

1.2. The beamsplitter assembly

Figure 3 is an exploded view of the beamsplitter assembly and Figure 4 a cross-section showing the critical components of the KBr mount. A center plate (part of the optical cell) creates the air-space wedge between the beamsplitter/combiner and the compensator elements. Together with the RTV face pads, the element spacing is also defined. The center plate is the major component of the optical cell. A beamsplitter (or compensator) cell wall and flange set are bonded to each side of the center plate to complete the optical cell. The center plate, walls and flanges are made from M55J graphite with a cyanate ester binder. Each component of the optical cell structure is bonded together with Hysol 9309.3 epoxy.

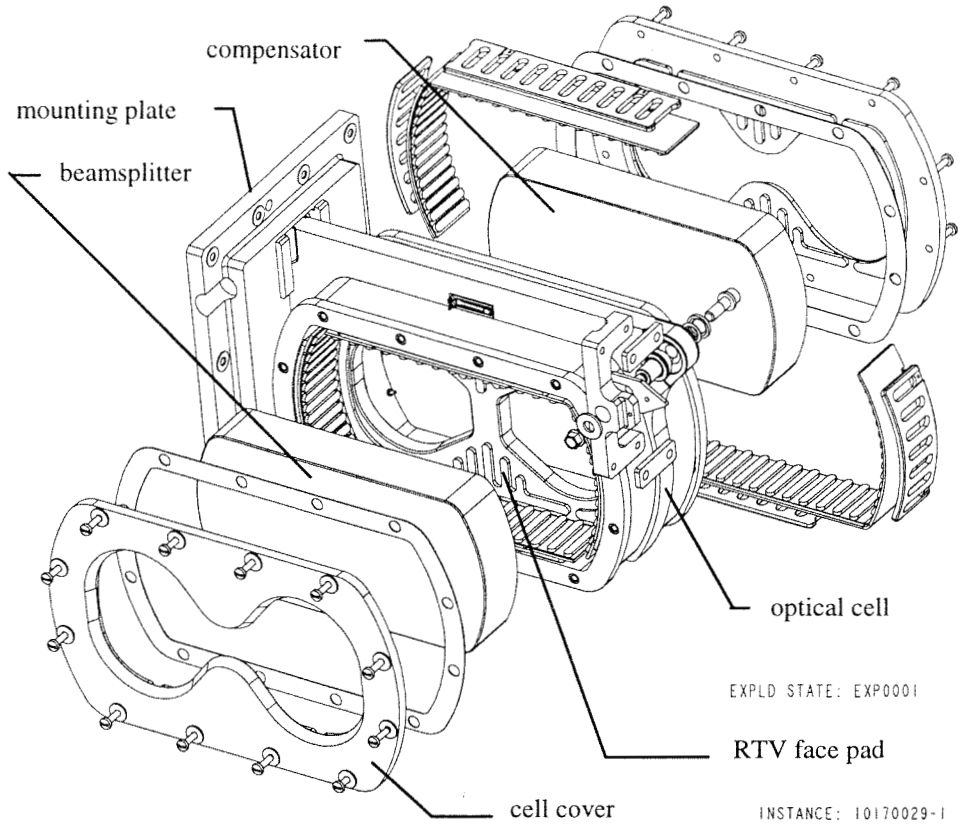

Figure 3. This exploded view of the TES Beamsplitter Assembly clearly indicates the primary structural and optical components. The optical cell, cell covers and mounting plate are each fabricated from graphite/cyanate ester lay-ups - the cell and plate from various pieces. Attachment hardware for the cell to the mounting plate are not visible.

The mounting plate is also a graphite/cyanate ester lay-up which includes sections of honeycomb for added lightness. It is bonded together from spars and face sheets using Hysol 9309.3 epoxy. The mounting plate provides two of the three attach point for the optical cell subassembly. A titanium bracket at the opposite side of the cell provides the third. Together, these attach points provide a kinematic, athermal, orthogonal and adjustable mounting scheme that is shimmed to achieve the required adjustment resolution.

The cell covers, as well, are made from the same graphite/cyanate ester and are bolted to the optical cell flange inserts at assembly. Aluminum L-shaped brackets with bonded RTV silicone pad strips are backed with aluminum shims and are used inside each optical cell cavity to support, isolate and lightly preload the optical elements along their edges.

The KBr beamsplitter/combiner and compensator element shape was fashioned after a 190 mm diameter disc, then, sections of the disc symmetrically removed resulting in a pseudo-rectangular shape 100 mm wide. Not reducing the KBr shape in this fashion would result in an additional 2 lbs. per optical element. This assembly consists of 7 lbs. of KBr and is currently calculated to be just under a total of 14 lbs..

The RTV silicone selected is a Nusil product, CV1-1142, and is an aerobic one-part sealant. It meets the low outgassing requirements for collected volatile condensable mass (CVCM) of <0.1% and total material loss (TML) of <1.0%. Table 1 lists the relevant material properties of this silicone as well as those of KBr and M55J graphite/cyanate ester. The face pads were designed to maintain as nearly as possible a high thickness to width ratio, maximize the KBr contact area and evenly distribute the contact area. The face pads are premolded and then bonded to the cell center plate and cell covers using the same RTV material and location fixturing.

Once each KBr optic is installed into the cell using special tooling, a cell cover is positioned, shimmed and preloaded to the appropriate deflection. The RTV face pads isolate the KBr optics from launch vibrations and later, provide a light preload to secure and maintain the desired position of the optics when at operating temperatures.

Other features of the mount approach are evident in Figures 3 and 4, however, they will not be completely addressed since the RTV face pads are the primary interest in this paper. The relevant design requirements are listed below in Table 2.

THERMAL	RTV	KBr	M55J Inplane	M55J Xplane
CTE (ppm/°C) (20oC->-110°C)	300*	41	-0.4*	56*
Tg (°C)	-113*		180	180
CVCM (%)	<0.01		<0.02	<0.02
TML (%)	<0.50		<0.10	<0.10
MECHANICAL				
Density(gm/cm3)	1.10	2.75	1.6	1.6
Elastic Modulus (psi)	~180*	3.9	20-24	20-24
Tensile Strength(psi)	250-375	160	--	8,000-10,000
Shear Strength (psi)	--	--	2,000 - 4,000	--
Compression Strength (psi)	--	--	--	43,000
Time-varying Strain @ 340#	5.5 %*	--	--	--
Stress relaxation	~14 %*	--	--	--

Table 1. Selected material properties for RTV CV1-1142, KBr and M55J graphite/cyanate ester. Values marked with an asterisk are measured. The KBr tensile strength value is actually its elastic limit and the RTV elastic modulus is an apparent value.

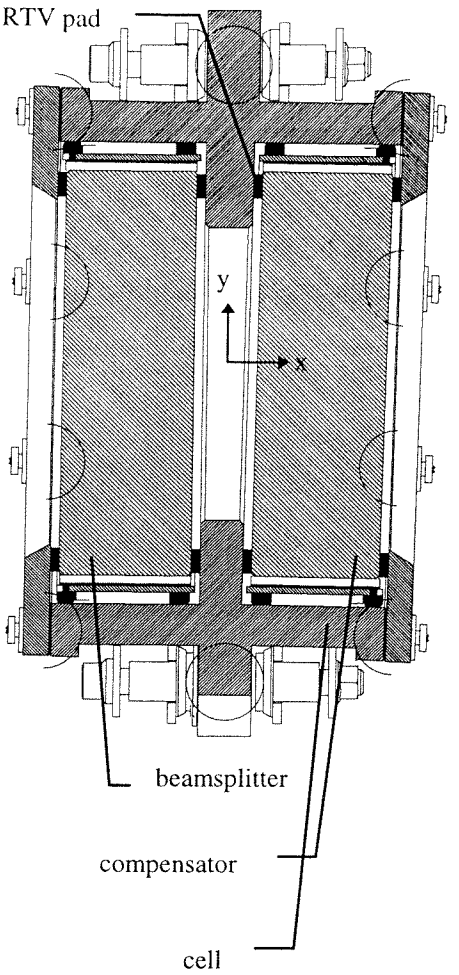

Figure 4. In this cross-section of the cell, the beamsplitter/combiner (left) and the compensator (right) cavities are shown with their respective KBr optical elements. The preloaded RTV face pads (black) are visible at two places either side of each optic. The cell covers clamp the KBr/RTV stacks against the optical cell center plate. The lateral preloading hardware is also visible but is better viewed in Figure 3.

Optical/Mechanical Design Requirements					
ENVIRONMENTAL	**Thermal**			**Vibration**	
	Design Range(°C)	-113 to +65		Random, 50-500 Hz (g2/Hz)	0.16
	Operating Range (°C)	-103 to -83			
OPTOMECHANICAL	**Mechanical**			**Optical**	
	*PISTON	*TILT	*TIP	KBr Wavefront (rms)	λ/10
Adjustment Range	± 2.5 mm	± 0.9°	± 0.6°	BS optic wedge	0.285°
Adjustment Resolution	± 0.0005 in. (0.013mm)	± 0.005° (20")	± 0.003° (10")	BS/Compensator relative wedge	0.861°
Thermal Stability	± 0.005 in.(0.13mm)	± 0.001° (4")	± 0.001° (4")	KBr Thickness, nom.	32 mm

* TIP is defined as rotation about the instrument y-axis, TILT about z and piston is along x as defined in Figure 1.

Table 2. Selected optical and mechanical design requirements for the TES beamsplitter assembly.

2. THE MOUNT APPROACH

RTV silicone was chosen to mount the KBr for various reasons. First, it had been used successfully in the Jet Propulsion Laboratory's (JPL) ATMOS project where the beamsplitter optic survived three shuttle launches. Second, the considerable mechanical hardware that other approaches[2,3] employed added mass to the system or functioned better with a circular optical element. Furthermore, analysis indicated that the ATMOS mounting technique could be extended to a cryogenic application if the appropriate RTV material properties (derived from test, see Table 1), configuration and preload (derived from the analytical model) could be selected to prevent overstressing the KBr during launch and at both bakeout and operating temperatures. Stability requirements (Table 2) could also be achieved if the RTV on either side of the optic were fabricated to spring rates within 10% of each other and control of RTV pad thickness were maintained within ± 0.005" over 7.5". Actual stability values at operating temperature ± 10°C have been calculated from the design geometry due to all error contributors as tip/tilt/piston of 1.0 arcsec/2.4 arcsec/36 μin. rms. Stability requirements were derived from detector pixel stability values for downtrack (36 arcsec) and crosstrack (3.6 arcsec) by transformation to the instrument coordinate system at the KBr optical surface. Refer to Figure 4 for the model description that follows.

2.1. The model

Initially, the TES RTV pads were scaled from the ratio of TES-to-ATMOS beamsplitter mass (~2.2:1). With 0.05" thick pads in ATMOS, TES required approximately 0.110" thick pads. Later, this model was developed to verify the feasibility of the approach and determine the best RTV pad geometry and preload. The RTV is modeled as a parallel, Hookean spring system for the launch case since the launch loads act inertially on the KBr mass. Although silicones exhibit viscoelastic behavior which is non-linear[4], using apparent elastic moduli with the measured load-deflection (L/D) curve (Figure 5) is a conservative assumption. To remove the time-varying strain within the RTV, the pads were permanently set using a load greater than the expected maximum launch load (360 lbs.). Material properties of the RTV were required as inputs to the model and were obtained through testing (see Table 1). The key properties required were the RTV coefficient of thermal expansion (CTE) over the range of 65°C to -108°C, the time-dependent strain - creep (to determine the RTV thickness after permanent set) and the apparent elastic modulus over the range of expected deflection. The model is composed of three constraint relationships.

The primary model constraint equation compares the sum of the initial RTV preload and the overall thermal contraction of the system (when going down to operating temperature) with that of the minimum compression required to maintain the optic in a 1g environment without slipping at the RTV interface. This is expressed as:

$$\delta_{preload} + \delta_{thermalCOLD} \geq \delta_{friction\text{-}1g,} \qquad (1)$$

In this expression, $\delta_{thermalCOLD}$ is a set of terms based solely on the design geometry where the CTE of KBr, RTV CV1-1142 and M55J graphite/cyanate ester are assumed constant. ΔT can be changed from -133°C to +45°C for use in evaluating the hot case (discussed later) where bakeout temperatures are an issue. Since two of these terms include the $\delta_{preload}$ term, it will be discussed next at greater length.

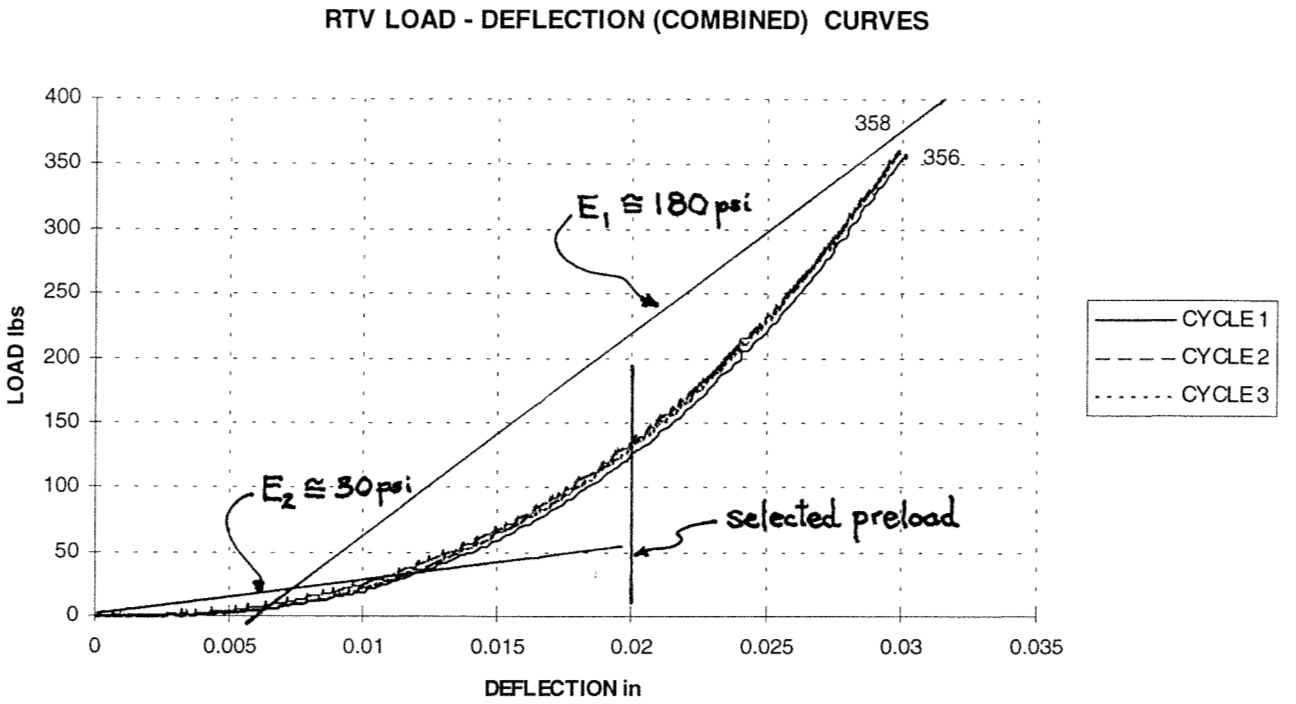

Figure 5. Measured Instron load-deflection data from 6.08 in^2 area of RTV pads, bonded to a graphite/cyanate ester plate with the same RTV as an adhesive. Prior to acquiring this data, the test sample was cured for 7 days, baked-out at 75°C for 72 hrs. then permanently set with a 360 lbs. static load for 5 days. The RTV apparent elastic moduli are also shown.

The $\delta_{preload}$ term is physically the result of compressing two RTV springs in series, however, a parallel equivalent spring model is used since the preload must be calculated to overcome the maximum expected deflection during shake. A factor ($n_{preload}$) is included to add varying margin to the actual preload value.

$$\delta_{preload} = (n_{preload})(WG)(L_{rtv}/2AE_1), \quad (2)$$

W is the optic weight (3.5 lbs.) and G is the expected acceleration in g's. $2AE_1/L_{rtv}$ is the $2*k_{rtv}$ for a parallel equivalent spring. The elastic modulus (E_1) for the deflection range in question was acquired from the test data. E_1 = 180 psi was chosen ultimately as the best estimate within the range of vibration deflection (see Figure 5). For thermal purposes, this relationship was also used in $\delta_{thermal}$ to calculate the new RTV pad thickness after preload compression.

Finally, the 1g friction term is given as:

$$\delta_{friction\text{-}1g} = (f/\mu)(2\, L_{rtv}/AE_2), \quad (3)$$

where E_2 = 30 psi was used from L/D data (Figure 5) when the RTV is under low strain conditions. Even at -98°C, preliminary L/D data demonstrated little change in E_2 at the low strain condition from data taken at room temperature. The friction coefficient for RTV against a smooth aluminum surface was measured to be approximately 1.5 to 1.7 and the friction force is the 1g weight of the optic. In this relationship, however, it was necessary to use the series equivalent spring for the RTV since this term is only applicable to the non-dynamic case and the preload is applied by the assembly covers.

Similar to Eqn. (1) for the low temperature extreme, the constraint equation for the case where the beamsplitter assembly must go through a 65°C (includes 5°C margin) bake-out is given as:

$$(\delta_{preload} + \delta_{thermalHOT})(E_1/2L_{rtv}) \leq n_s * \sigma_{limit,} \quad (4)$$

$\delta_{preload}$ and $\delta_{thermalHOT}$ are identical expressions to those in Eqn. (1) except that $\delta_{thermalHOT}$ uses ΔT = +45oC. σ_{limit} is the elastic limit of KBr (see Table 1) and n_s (set at 0.75) is a safety factor to provide adequate margin from KBr deformation failure. The equation assumes a series equivalent spring since thermal expansion is not a dynamic condition and is considered similar to adding preload.

Finally, the dynamic constraint case is given as:

$$(\delta_{preload} + \delta_{oscill})(2E_1/L_{rtv}) \leq n_s * \sigma_{limit,} \quad (5)$$

Again $\delta_{preload}$ is identical to that given in Eqn. (2). However, δ_{oscill} is the actual maximum oscillating deflection of the KBr element under load and is expressed as:

$$\delta_{preload} = (n_{preload})(WG)(L_{rtv}/2AE_1), \quad (6)$$

The only difference between δ_{oscill} and $\delta_{preload}$ is the margin factor ($n_{preload}$) added to $\delta_{preload}$ to assure positive preload of the optic during launch. Since this is a purely dynamic expression, the RTV equivalent spring is modeled as parallel.

2.2. Model results

Solving Eqns. (1) and (4) for L_{rtv}, results in two expressions where $L_{rtv(COLD)}$ and $L_{rtv(HOT)}$ are each greater than a collection of known or derived variables. The result of these constraint equations are plotted at several g levels and values of E_1 in Figure 6. If the beamsplitter assembly is considered similar to structure (rather than a component subject to Miles equation acceleration estimates - 99 g's max.), a Delta II rocket mass acceleration curve (MAC) gives the maximum expected g level for the beamsplitter assembly of 77 g's (includes a limit load factor of safety of 1.4). Figure 6 plots L_{rtv} for 65, 75 and 85g's (approximately $\pm$10g min./max. limit about 77g's) and for the best estimated range of RTV apparent modulus (150-210 psi). Predicted deflection of the KBr optics under worst case vibration load is predicted by the model as $\pm$ 0.015" at 85g and 180 psi modulus. The model predict for operating temperature preload under the same conditions is 0.007". Although the L_{rtv} COLD curve in Figure 6 indicates an L_{rtv} of ~0.180", this turns out to be mitigated by accepting a slightly higher limit stress in the optic than 120 psi and fixing the preload term in the constraint equations to a constant (this is discussed further shortly).

In solving Eqn. (5), the L_{rtv} term drops out and an expression for RTV area can be derived:

$$\text{RTV Area} \geq (n_{preload} + 1)(WG/ n_s \sigma_{limit}), \quad (7)$$

This relationship results in an expression that gives a low limit to the proper RTV area needed to prevent KBr overstress at varying g levels. These are plotted in Figure 7. The stress limit plotted ($n_s \sigma_{limit}$) is for 120 psi maximum (n_s =0.75).

Eqn. (1) and (4) constraints also provided a means of estimating the proper preload that avoids KBr overstress and a zero preload condition at operating temperature. These values were 0.017", 0.020" and 0.022" at 65, 75 and 85 g's, respectively. A preload of 0.020" nominal was selected and the derived L_{rtv} relationships from Eqns. (1) and (4) and Eqn. (7) were rewritten to solve for KBr stress. A target apparent modulus of 180 psi and RTV area of 6.05 in^2 were used in the rewritten expressions to obtain the results plotted in Figure 8. In the target apparent modulus region, even up to slightly higher than 190 psi, the worst case KBr stress is below the 120 psi desired maximum.

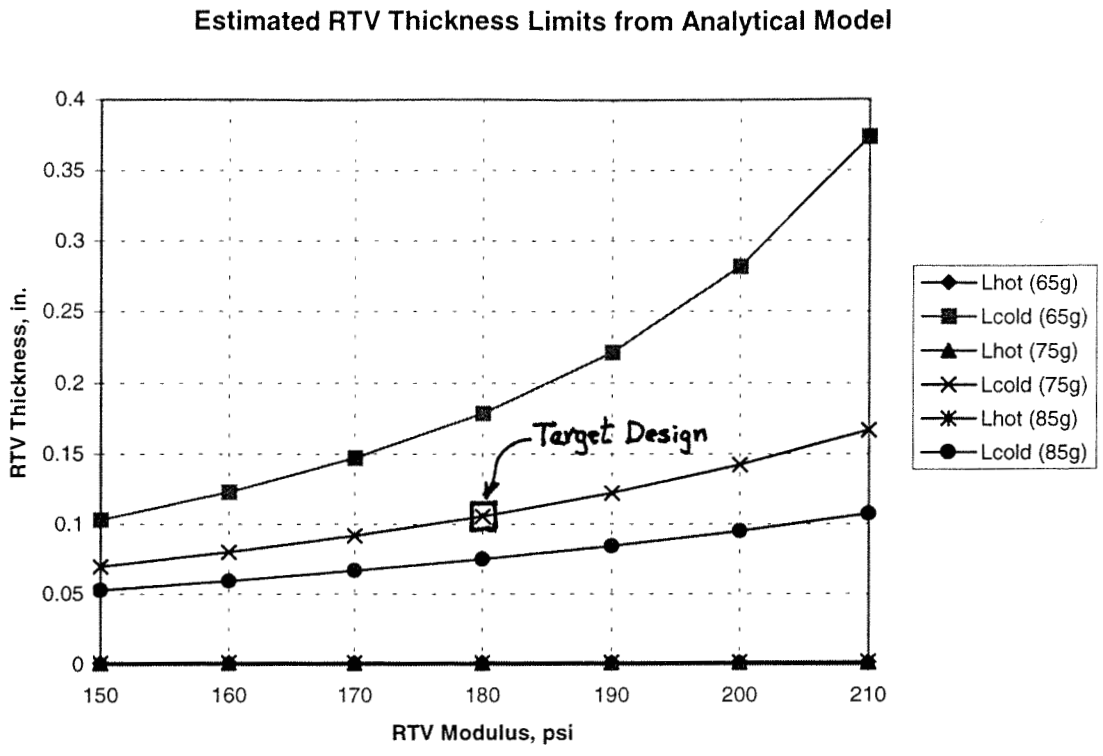

Figure 6. Lhot and Lcold are the L_{rtv} values plotted for the HOT and COLD constraint Eqns. (4) and (1), respectively. The three different HOT case relationships each produced very similar values and are nearly superimposed at the bottom of the graph. The target design L_{rtv} (=0.110") and apparent modulus (=180 psi) are indicated by the large square.

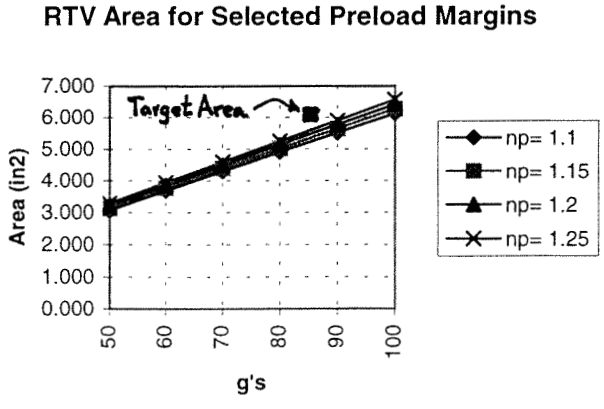

Figure 7. Plot of RTV required area for a given preload margin over a range of possible g levels. Increasing preload margins increases the required area for a given g level. At a 25% margin, even at the 85 g level, the current target design RTV area (6.05 in^2) exceeds the minimum (5.6 in^2) determined from constraint Eqn. (7).

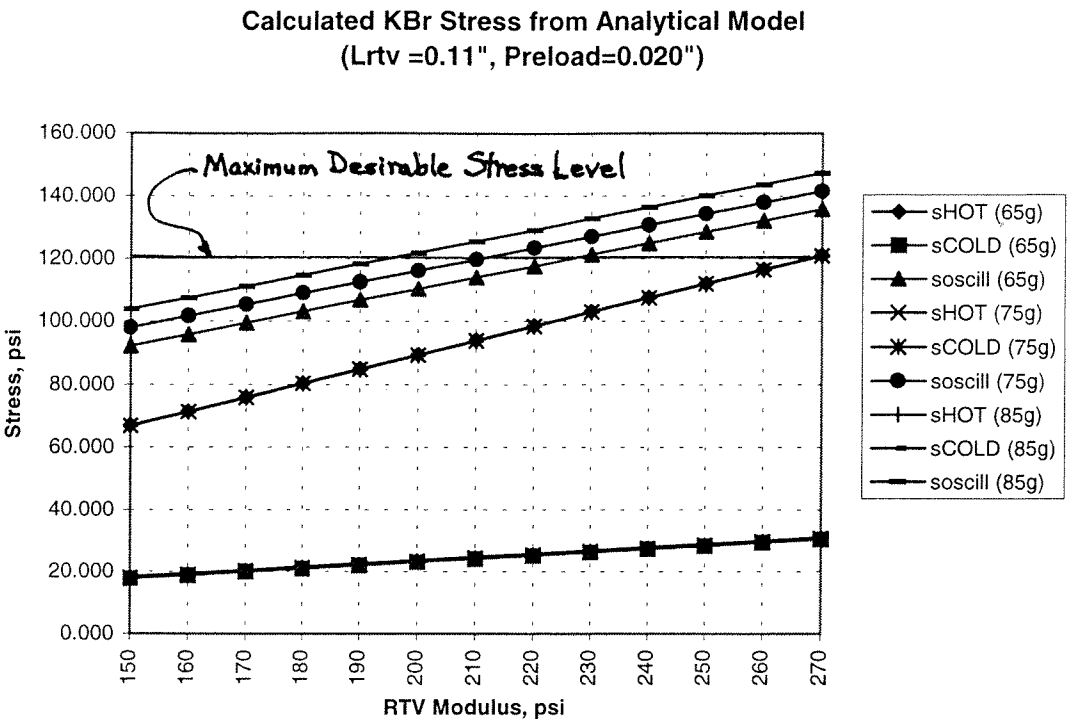

Figure 8. Plot from results of the analytical model showing predicted stress levels in the KBr optics at various g levels and over a range of possible RTV apparent moduli. The dynamic oscillation case given by Eqn. (7) for the three values of g's are sufficiently separated at the top of the plot. The three HOT case curves are very nearly superimposed to be indiscernible from one another. Likewise, the COLD case curves are superimposed at the bottom of the plot.

3. CONCLUSION

Although still no data is available from thermal and vibration testing of the beamsplitter assembly development unit, an analytical model and preliminary structural models of the entire assembly have been performed and have yielded promising results. Preliminary structural modeling resulted in estimates of the KBr stress under vibration loads (without preload), of 51 psi. The selected, nominal preload of 0.020" will produce approximately 54 psi more stress in the KBr resulting in a total of 105 psi compared to the maximum model result (at 180 psi apparent RTV modulus) of 115 psi (~10% error).

The nominal area of RTV-to-KBr contact is currently 6.05 in^2 and the RTV mold has produced pads with thickness variations no greater than $\pm$ 0.003". The RTV area has been controlled by the mold process to easily less than 1%. If the RTV bonding process can control the overall thickness tolerance to $\pm$ 0.005", the success of this design based on the model predictions is assured.

One other issues remains, however, pertaining to the RTV stress relaxation behavior[5]. Test data presented in Table 1 indicate that under constant deflection, the RTV will reach a maximum load at initial application, then, relax approximately 14%. There remains the question that, when at operating temperature, will the remaining preload deflection really be the 0.007" value quoted earlier such that the optical elements do not slip and loose alignment from the installed position? Since it will take approximately 14 hrs. to get to operating temperature from room temperature, it is possible that the RTV will go through some recovery as well (typically about 1.5% over a 24 hr. period as measured in test). The results from the development unit thermal and vibration testing is expected to resolve this issue.

4. ACKNOWLEDGEMENTS

I want to thank the many others who made this paper possible. Mitch Ruda and Kevin Sawyer of Ruda and Associates and Dave Miller of the Jet Propulsion Laboratory (JPL) provided excellent review and support of and attention to the details of the design as it progressed. Drawings of the optical bench, interferometer and beamsplitter assembly views were provided by Eric Roybal of JPL from ProE CAD files. Paul Willis (JPL) provided literature on the behavior of viscoelastic materials, RTV test planning support and review of RTV test data and the related text in this paper. Dave Rider, also of JPL, provided accurate technical descriptions of the TES mission and purpose. The research described in this paper was conducted by the Jet Propulsion Laboratory, California Institute of Technology, under a contract with the National Aeronautics and Space Administration.

5. REFERENCES

[1] EOS, TES Science Objectives & Approach, Goals & Requirements, JPL Document, D-11294, Rev 5.0, dated 24May1996

[2] Hagopian, J. G., Hayes, P., Crooke, J., Lyons, J., Morell, A., French, T., Hersh, M., Lashley, C., Schmidt, S., "High-stability, adjustable, cryogenic-compatible beamsplitter mounts for the Composite Infrared Spectrometer (CIRS) for the Cassini mission to Saturn", *Proceedings of the SPIE - The International Society for Optical Engineering Conference*, Vol. 2814/81-91, SPIE - Int. Soc. Opt. Eng., 1996

[3] Kemp, J. C., Wellard, S. J., Goode, D. C., Huppi, E. R., "Cryogenic Michelson interferometer spectrometer for Space Shuttle application", *Proceedings of the SPIE - The International Society for Optical Engineering Conference*, Vol. 686/151-159, SPIE - Int. Soc. Opt. Eng., 1986

[4] "Designing for rigidity and strength under static load", *Modern Plastics Encyclopedia*, McGraw-Hill, Vol. #63/No.10A, pp. 403-411, McGraw-Hill, New York, 1986-87

[5] "Designing and selecting plastics for stress relaxation", *Modern Plastics Encyclopedia*, McGraw-Hill, Vol. #63/No.10A, pp. 428-432, McGraw-Hill, New York, 1986-87